J. Phys. G: Nucl. Phys. **13** (1987) 297–310. Printed in the UK

π^-p bremsstrahlung at 300 MeV/c

The Omicron collaboration:
S M Playfer†[a], W van Doesburg‡[b], A G Zephat‡[c], T Bressani§[d], E Chiavassa‖, S Costa‖, J D Davies†, G Dellacasa‖, C W E van Eijk¶, M Gallio‖, R W Hollander¶, J V Jovanovich£, G Kernel$, W Lourens¶, J Lowe†, E G Michaelis††[e], A Musso‖, F Sever$, F Siohan‡‡[f], A Stanovnik$ and N W Tanner‡‡

† Physics Department, University of Birmingham, Birmingham B15 2TT, UK
‡ Physics Department, Free University, Amsterdam, The Netherlands
§ Dipartimento di Scienze Fisiche, Universita di Cagliari, 09100 Italy
‖ Istituto di Fisica Superiore dell Universita, Corso Massino d'Azeglio 46, I10125, Torino, Italy
¶ Physics Department, Technische Hogeschool Delft, c/o IRI, Mekelweg 15, Delft, The Netherlands
£ Department of Physics, University of Manitoba, Winnipeg, Manitoba R37 2N2, Canada
$ Jozef Stefan Institute and Department of Physics, E Kardelj University, Ljubljana, Yugoslavia
†† CERN, Geneva 23, Switzerland
‡‡ Nuclear Physics Laboratory, Keble Road, Oxford OX1 3RH, UK

Received 20 March 1986, in final form 6 August 1986

Abstract. Cross sections are presented for the reaction $\pi^-p \to \pi^-p\gamma$ at $\sqrt{s} = 1234$ MeV.

1. Introduction

Several previous studies of the bremsstrahlung reaction, $\pi p \to \pi p\gamma$ at incident pion momenta of a few hundred MeV/c have been made with a view to improving our understanding of the π–nucleon interaction in the region of the $\Delta(1236)$. There are at least two areas in which the bremsstrahlung process is potentially able to yield information relevant to this.

(i) If the bremsstrahlung takes place by 'external emission', i.e. by radiation from one of the external lines in the graphs of figure 1(*a*), then the π–p interaction at the vertex is off-shell, and the bremsstrahlung process may give information on the off-shell behaviour of the pion–nucleon interaction.

[a] Present address: SIN, Villigen, Switzerland.
[b] Present address: Elektrizitäts-gesellschaft, Laufenburg AG, Zürich, Switzerland.
[c] Present address: Philips, Eindhoven, The Netherlands.
[d] Present address: Istituto de Fisica Superiore dell Universita, I10125, Torino, Italy.
[e] Present address: Nuclear Physics Laboratory, Keble Road, Oxford OX1 3RH, UK.
[f] Present address: CERN, Geneva 23, Switzerland.

0305-4616/87/030297 + 14 $02.50

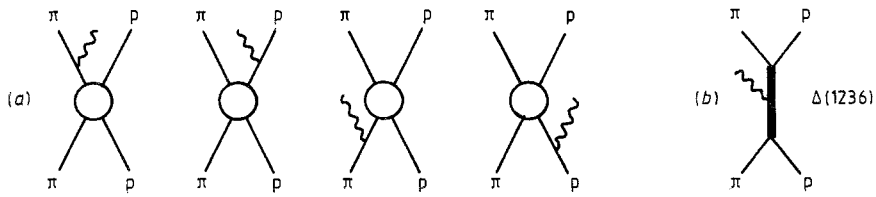

Figure 1. Processes which can contribute to π–p bremsstrahlung; (*a*) 'external emission' graphs, and (*b*) 'internal' radiation from the $\Delta(1236)$.

(ii) Near the $\Delta(1236)$ itself, the graph shown in figure 1(*b*) is expected to contribute significantly to the process. The contribution from this term will depend on the magnetic moment of the $\Delta(1236)$, specifically for the Δ^{++} in the case of π^+p bremsstrahlung and the Δ^0 for π^-p bremsstrahlung.

Several experiments were carried out in the 1970s by the UCLA group [1–5]. In their earlier experiments [1–4] the incident pion energy was chosen above that of the $\Delta(1236)$ and, in an attempt to observe the process in figure 1(*b*), an enhancement in the bremsstrahlung yield was sought for photon energies such that the final π–p system had the energy of the Δ. No such effect was observed in any of their experiments. In later experiments [5] an initial energy on the $\Delta(1236)$ was used. For most energies, both π^+ and π^- beams were used in an attempt to isolate the effect of the $\Delta(1236)$; the SU(6) prediction is that the Δ^0 should have zero magnetic moment while the Δ^{++} has twice the proton magnetic moment. Because of this, any effect of the $\Delta(1236)$ should be much more pronounced for π^+p than for π^-p bremsstrahlung. Again, no evidence for the effect of the $\Delta(1236)$ was found.

The situation regarding the theoretical understanding of the bremsstrahlung process is not clear. The earliest attempts were based on the work of Low [6] which was applied to the UCLA data by Sober *et al* [2]. They used only the first two terms in the expansion derived by Low and referred to the model as the soft-photon approximation (SPA). For low photon energies, <40 MeV, the SPA predicts a $1/k$ dependence of the cross section, in reasonable agreement with the data. For higher photon energies, a sharp rise in yield, predicted by the SPA, was not observed; however, the SPA is not expected to be valid at these energies. Liou and Nutt [7] were able to fit π^+p bremsstrahlung using a modified version of the SPA.

Picciotto [8–10] has attempted to extract parameters related to the off-shell π–N interaction from bremsstrahlung data, and has obtained a reasonable fit to the π^-p results of reference [1].

Attempts to deduce the $\Delta(1236)$ magnetic moment by calculating the contribution from figure 1(*b*) were made by Kondratyuk and Ponomarev [11] and by Fischer and Minkowski [12]. Both these calculations predicted a peak in the photon spectrum from π^+p bremsstrahlung, in contrast to the monotonic decrease observed experimentally. This observation is in line with the situation noted above, that the $\Delta(1236)$ does not appear to influence the bremsstrahlung in the expected way. In a later calculation, however, Pascual and Tarrach [13] suggested that the observed monotonic photon spectrum could result from a cancellation involving the contribution from the $\Delta(1236)$, and that the experimental results can be understood if the Δ^{++} has exactly the magnetic moment predicted by SU(6). However, it seems that this theory could not simultaneously describe the π^-p data.

A surprisingly good fit to both π^+ and π^- data was obtained by Nefkens and Sober [14] using just the external emission graphs of figure 1(*a*) and taking only the first term

Table 1. Summary of recent π–p bremsstrahlung data.

p_π(lab.) (MeV)	T_π(lab.) (MeV)	$\sqrt{s}$ (MeV)	π^-p data	π^+p data
442	324	1330	[4]	[4]
412	298	1312	[2, 3]	[2, 3]
384	269	1291	[4]	[4]
301	192	1234	Present work	—
271	165	1213	—	[5]

from the formalism of Low [6]. This procedure, referred to as external emission dominance (EED), gives good fits to both energy and angle dependence of the cross section. However, it is not at all clear why such a simplified treatment should produce good fits, particularly since the more complete treatment, the SPA, is less successful.

The theoretical situation, then, is unsatisfactory in that, although acceptable fits to experiment have been obtained in a few cases, there is no overall picture that can fit data for all momenta and both charge states. Further, the best fit seems to be provided by the simplest model and it is curious that improvements to some models may result in a worse fit. Recently, at least two groups have approached the problem again [15, 16] and one can hope for further insight in the near future.

In the present paper, experimental results are presented for measurements of π^-p bremsstrahlung at a laboratory momentum of 301 MeV/c $\sqrt{s}=1234$ MeV. The data complement those of the UCLA group in providing information near the $\Delta(1236)$; table 1 summarises the measurements taken by that group and in the present work. Our experiments differed from those of the UCLA group in that the photons were not detected. Instead, the final-state charged particles were observed and a kinematic reconstruction of events identified emitted photons. The measurements were performed in parallel with a study of e^+e^- pairs from π^-p interactions [17].

2. Experimental method

The experiments were carried out with the Omicron spectrometer [18, 19] using a π^- beam provided by the CERN synchro-cyclotron. More detail can be found in the account of the parallel e^+e^- experiments [17]. Figure 2 shows the arrangement of chambers, target and counters within the magnetic field which served to analyse the momenta of the ingoing beam particles and of the charged secondaries. The magnet provided a region of approximately uniform magnetic field in a $2 \times 1 \times 0.85$ m^3 gap, with a central value of 0.5095 T for the present experiments. The field was surveyed to 0.1% accuracy and parametrised in terms of coefficients of Legendre polynomials for subsequent use in analysis programmes [20, 21]. The experimental procedure and a preliminary version of the results have been described elsewhere [21].

The 301 MeV/c pion beam was obtained with 0° production by 600 MeV protons incident on a 10 cm thick Be target. In order to obtain a useful beam intensity of about 10^6 particles/s it was necessary to use a momentum band of 6% FWHM. The residual dispersion and scattering in the detectors upstream of the target resulted in a beam spot of 48 mm width and 40 mm height (FWHM). Measurements with gas Čerenkov counters and time-of-flight techniques (see, e.g. Zavrtanik *et al* [22]) showed that the beam consists of 72% π^-, 20% e^- and 8% μ^-. The beam momentum distribution shown in figure 3 was measured

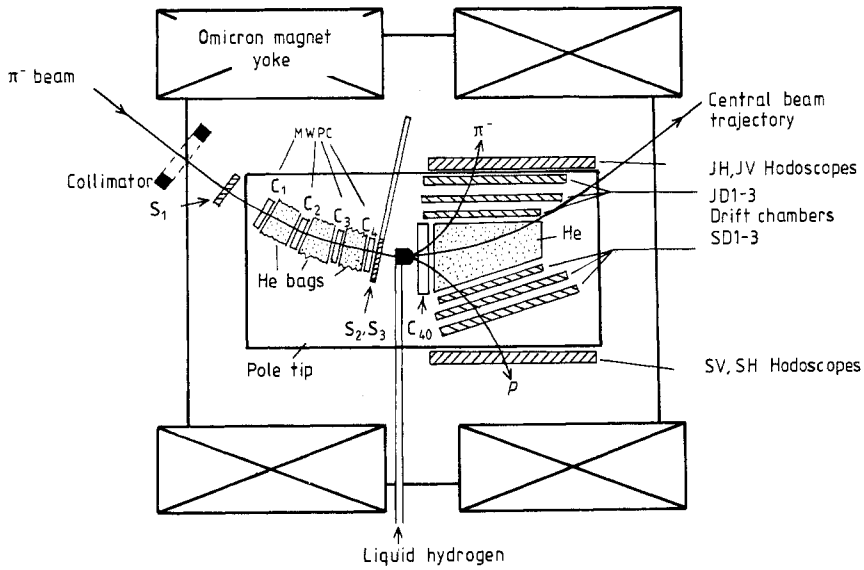

Figure 2. The arrangement of detectors and the target in the Omicron magnet.

with the spectrometer during the experimental runs. The cyclotron duty cycle was typically 50% during the experiments.

The following detectors, shown in figure 2, were used in the spectrometer.

(i) Scintillators S1 and S2 and a halo–veto counter, S3 to define the incident beam.

(ii) Multiwire chambers C1–C4 to track beam particles to the target. Each chamber had planes of vertical and horizontal wires of 1 mm pitch, and, in addition, C1 and C4 had diagonal wires.

(iii) A multiwire chamber C40 with four planes (vertical, horizontal and two diagonal) to detect secondary particles leaving the target.

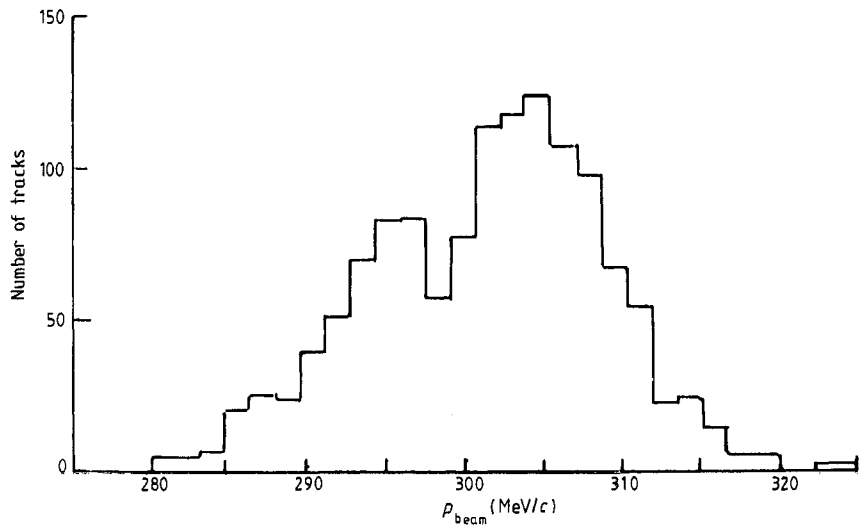

Figure 3. The beam momentum distribution.

(iv) Six drift chambers JD1-3 and SD1-3, each with planes of vertical and horizontal wires, to track secondary pions and protons respectively.

(v) Vertical and horizontal hodoscopes, JV, JH, SV and SH, behind the last drift chamber in each secondary arm.

Some of the spaces between the chambers were filled with He bags. The detector assembly was mounted on an aluminium plate which could be withdrawn from the magnet to enable the chamber positions to be surveyed. Detailed descriptions of the chamber design have been given elsewhere [17, 23, 24].

The trigger was defined by the scintillators as

$$S1_{\wedge}S2_{\wedge}\overline{S3}_{\wedge}JV_{\wedge}JH_{\wedge}SV_{\wedge}SH$$

where JV, JH, SV and SH indicate a signal in any element of the respective hodoscope plane. This trigger therefore requires at least one charged particle in each arm. Since the scintillators SH and SV were used to detect low-momentum protons, their discriminators were set high enough to suppress, as far as possible, pulses from minimum-ionising particles. In addition, a sample of beam triggers, defined by

$$S1_{\wedge}S2_{\wedge}\overline{S3}$$

was also recorded.

Problems were encountered during the experiment with a high rate of spurious triggers resulting from electrons in the beam. Electrons can produce showers that yield enough secondary charged particles to trigger both hodoscopes. Two methods were used at various times to overcome this problem.

(i) A threshold gas-Čerenkov counter was inserted in the beam, before S1, to veto electrons; and

(ii) Since the secondary particles generated by electron-induced showers lie close to the median plane of the spectrometer, events were rejected if only the median-plane elements of the hodoscopes JH and SH were triggered. This 'central-plane veto' provided a substantial reduction in electron-induced triggers while losing only 12% of genuine triggers.

A sample of triggers was recorded in which the central-plane veto was not imposed.

For each valid trigger, data from all detectors were read via a Camac interface into a HP21MX on-line computer. From this computer, data were written to tape for subsequent analysis using the 3081D-ATLAS 10 computers at the Rutherford Appleton Laboratory. Several target-empty runs were interspersed in the data taking. Also, some cosmic-ray runs were taken with the beam counters removed from the trigger, to provide alignment and efficiency calibration for the drift chambers and hodoscopes.

3. Track analysis

For each arm (beam, proton and secondary pion) separately, hits in wire and drift chambers were associated into tracks by a pattern recognition technique. This track-finding process was found to be reasonably reliable except when two or more beam tracks were present, in which case the procedure was sometimes unable to sort the hits correctly into separate tracks. To avoid possible errors from this, all events with more than one beam track were rejected, giving a 15% loss of good beam tracks.

After the track finding, a least-squares fit to the hit coordinates on each track was then made using the full magnetic field map. For each track, the fitted momentum and position at the target boundary were recorded along with the goodness-of-fit parameter (χ^2).

In the third stage of the analysis, a vertex fit was performed. Each track was represented by its parameters at the target boundary and a vertex position was determined by a least-squares fit to these parameters, making due allowance for energy loss in the target.

The performance of the analysis chain was monitored by a simulation programme in which Monte-Carlo generated events were subjected to the same analysis procedures as described above for data events. The analysis of simulated events was used to determine the acceptance of the apparatus as well as to check the efficiency of the analysis procedure. To ensure that the simulation programme gave an accurate value of the acceptance, the effects of scattering by chamber and target materials were included in the programme as was the possibility of pion decay. Also, since the acceptance depends on the interaction point in the target, Monte-Carlo events were generated starting from parameters of actual beam tracks, deduced by fitting tracks from the beam sample trigger.

The following inefficiencies and losses were found in the analysis procedure.

(i) Events with multiple secondaries that could not be reconstructed, a loss of 3.7%.

(ii) 15% of good events lost by the χ^2 cut (see § 4). The uncertainty in the number of genuine events lost was estimated from the shape of the probability distributions to be 20% of that number. Thus the correction factor is 0.85 ± 0.03.

(iii) Faulty tape buffers written by the on-line system lost 2% of events.

(iv) The efficiency of the hodoscopes was determined from analysis of cosmic-ray tracks. A trigger was set up in which cosmic rays were identified by drift chambers placed close to the hodoscopes. By observing the fraction of such tracks that triggered the hodoscopes, the combined hodoscope efficiency was found to be (0.905 ± 0.010). Corrections for these were made in the evaluation of the cross sections.

The incident pion flux was measured during the experiment by scaling the beam triggers, $S1_A S2_A \overline{S3}$ and correcting this for the following factors.

(i) The beam composition. As mentioned in § 2, the beam consists of 0.20 e^-, 0.08 μ^- and 0.72 π^-. Several determinations of this have been made (see, e.g. reference [22]), and in addition, those runs in the present experiment in which a Čerenkov counter was used in the beam provide a further measurement of the electron component. The error is estimated from the reproducibility of the various measurements giving a pion component of 0.72 ± 0.03. Due allowance was made for the Čerenkov counter for those runs in which it was used in the trigger.

(ii) The beam track-finding and fitting efficiency, a correction of 0.74. Losses at this stage are due mainly to chamber inefficiencies and noise hits. The fluctuation from run to run is about ± 0.05. This is just outside statistics and probably represents the variation in chamber efficiency due to changes in the incident beam flux. As a precaution to allow for any possible differences between fitted and unfitted beam tracks, this error has been doubled, giving a correction of 0.74 ± 0.10.

(iii) A beam momentum cut of $270 < P_{\text{beam}} < 330$ MeV/c was applied to eliminate scattered particles and wrongly associated hits. A fraction 0.91 ± 0.01 survived this cut.

(iv) As mentioned above multiple beam tracks were excluded giving a correction of 0.85 ± 0.01.

(v) A fraction 0.79 of beam tracks intersected the target, determined by tracking fitted beam tracks through the magnetic field.

4. Results

Figure 4 shows the distribution of vertices in the target from both target-full and target-empty runs. In the 'target-empty' runs, the target vessel in fact still contained gaseous hydrogen at a temperature close to its boiling point. The target walls are clearly visible in

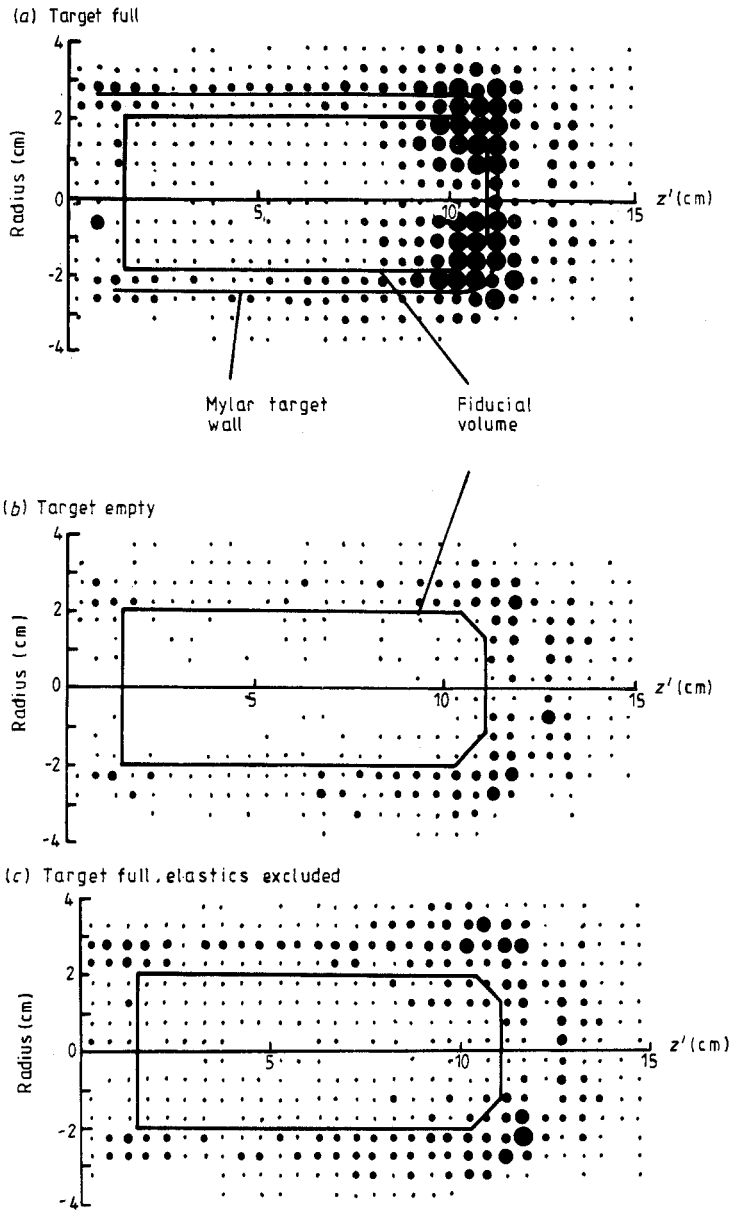

Figure 4. Distribution of vertices in the vicinity of the target, (*a*) with the target full, (*b*) with the target empty and (*c*) with the target full but for inelastic events only. The density of vertices is represented by the size of the points. The coordinate z' is along the long axis of the magnet.

the target-empty distribution, and events in the fiducial volume shown were selected. The event rate with target empty was 1.6% of that with the target full when normalised to the same incident pion flux. This is reasonably consistent with the ratio of the densities of gaseous and liquid hydrogen, and confirms that contamination from target-wall events is negligible.

The most prolific process in the target is π–p elastic scattering. Such events are only just within the geometrical acceptance of the apparatus, a feature which gives rise to the high density of vertices at the downstream end of the target, evident in figure 4(*a*). For the same reason, elastically scattered particles are confined to the upstream ends of the drift chambers. As a result of this, the range of π–p opening angles is restricted to about $(108 \pm 3)°$. This fact, together with the co-planarity requirement, enables elastic scatters to be identified readily. Figure 4(*c*) shows the distribution of vertices for a sample of events in which elastic scatters are excluded, which results in a more uniform distribution throughout the fiducial volume.

Figure 5 shows a plot of the missing energy,

$$\Delta E = E_\pi + m_p - (E_{\pi'} + E_{p'})$$

where primed quantities refer to final-state variables, for a sample of elastic scatters. The distribution has a FWHM of 23 MeV. This gives a measure of the energy resolution for elastic scattering, which is limited in this experiment mainly by multiple scattering of the secondary particles which results in errors in the momentum determination. By contrast with elastic scatters, bremsstrahlung events are distributed more uniformly over the target and the drift chambers.

Candidate bremsstrahlung events were then selected by imposing the fiducial volume cut shown in figure 4 and also a cut on goodness of fit. For the latter, a combination of χ^2 cuts for the individual tracks and for the vertex fit was used. The combined effect was a loss of 15% of good events. Bremsstrahlung events were then selected by plotting the

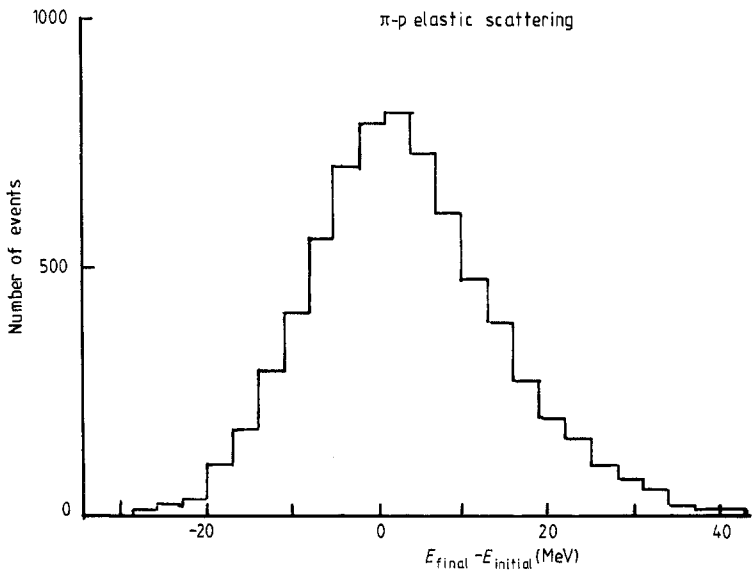

Figure 5. The distribution of missing energy for elastic scattering events. The density of events is represented by the size of the points.

missing energy, ΔE, against the missing momentum,

$$\Delta p = |\boldsymbol{p}_\pi - (\boldsymbol{p}_{\pi'} + \boldsymbol{p}_{p'})|.$$

For bremsstrahlung events, $\Delta E = \Delta p$. Figure 6 shows a scatter plot of ΔE and Δp for those bremsstrahlung candidate events that satisfy the angular restrictions discussed below. The events show a distinct clustering around the photon line. Figure 6 also shows the lines on which pion production events,

$$\pi^- p \to \pi^- p \pi^0$$

will lie. The small number of events seen around this line may arise from this process. However, no cross section can be extracted since the beam momentum is only just above threshold for pion production; the low-energy protons can only reach the hodoscopes if the production takes place in the downstream end of the target.

Two other types of event can contribute to figure 6. If, after an elastic scatter, the outgoing pion or proton subsequently scatters off a proton or a heavier nucleus, energy and momentum will be carried away by this nucleus. If the scattering is through a small enough angle and is reasonably close to the first scattering vertex, the event may still pass the vertex reconstruction. In this case, ΔE and Δp will be the energy and momentum of the unobserved recoil nucleus. Thus $\Delta E \ll \Delta p$ and events will lie close to the Δp axis. Such events can be seen clearly in figure 6. They do not contaminate the bremsstrahlung region for $\Delta E > 50$ MeV.

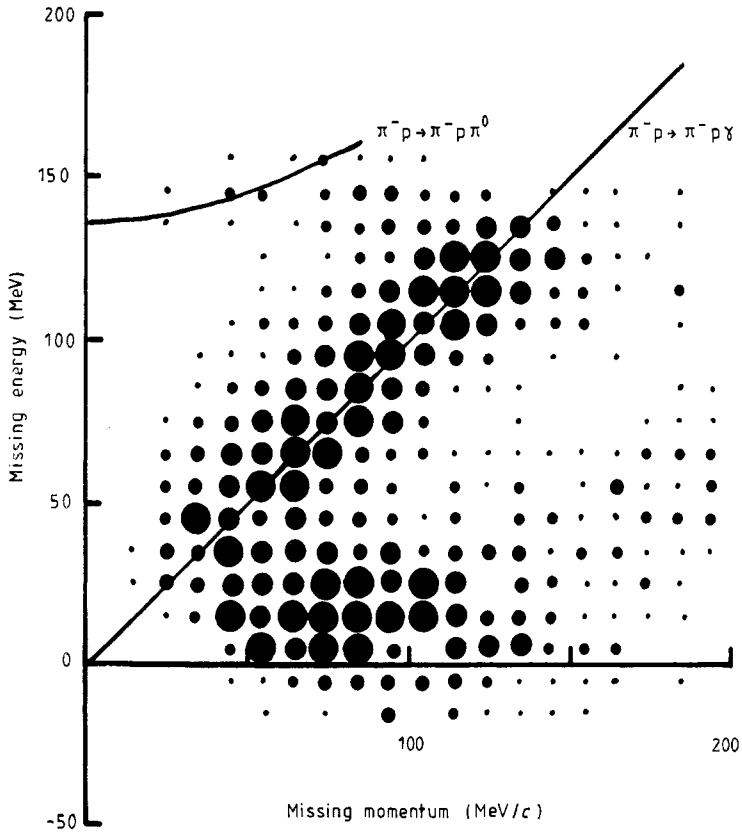

Figure 6. Plot of missing energy against missing momentum.

The remaining possible contaminant event is a π^-p elastic scatter followed by a π decay; again if this decay occurs sufficiently close to the scattering vertex the event may pass the vertex reconstruction. In this case, ΔE and Δp are approximately the energy and momentum of the decay neutrino. The probability of such a decay is rather low, but in any case, these events do not contaminate the bremsstrahlung region because they mostly result in forward-going neutrinos, whereas bremsstrahlung cross sections are given for $\theta_\gamma \geqslant 90°$ (see below). For those decays for which $\theta_\nu > 90°$ the neutrino energy is low and the corresponding ΔE is less than 50 MeV.

The bremsstrahlung signal is shown more quantitatively in figure 7, in which the distribution of $(\Delta E - \Delta p)$ is plotted for all events in figure 6 for which $\Delta E \geqslant 40$ MeV. The background is clearly small. The FWHM of this distribution is 35 MeV. Also shown in figure 7 is the corresponding plot for simulated events, for which the FWHM is 27 MeV. These values are reasonably consistent, and the slightly larger value found experimentally presumably reflects the effects of minor chamber misalignments and other features not included realistically in the simulation programme.

The bremsstrahlung cross section is a function of five independent variables; there are two angles and a momentum each for the scattered pion, the proton and the gamma ray and these are related by four kinematic constraints implied by four-momentum conservation. For the present experiment the five independent variables chosen are the

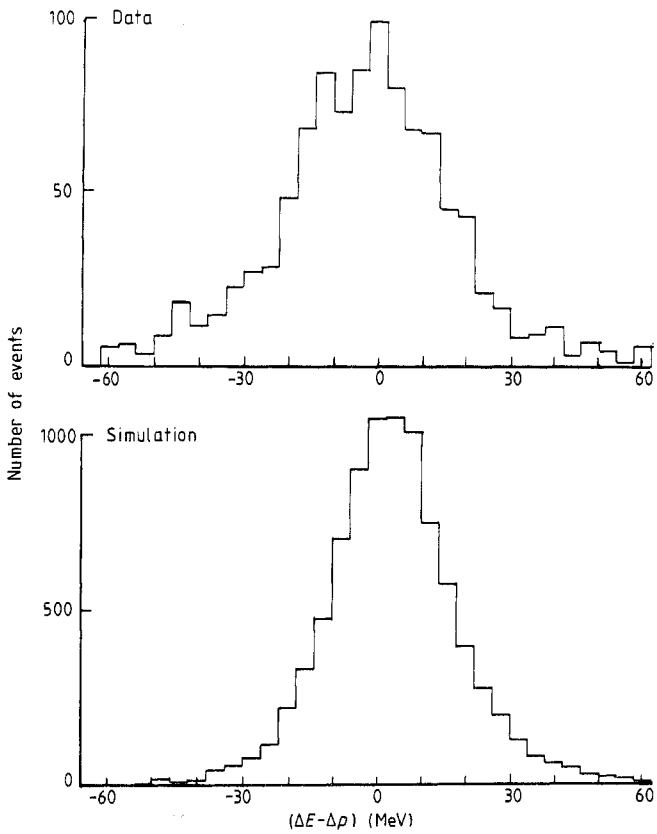

Figure 7. Distribution of $(\Delta E - \Delta p)$ for bremsstrahlung candidates and for simulated bremsstrahlung events.

three centre-of-mass gamma-ray variables, k, θ_γ^* and φ_γ^* and the pion centre-of-mass angles θ_π^* and φ_π^*.

Although the experiment is sensitive to a wide range of gamma-ray variables, only a limited angular range was covered for both the pion and the proton. For the pion, this restricts the range of θ_π^* and φ_π^* covered and the cross section quoted below is an average over a finite angular range. Since the proton angles have not been chosen as independent

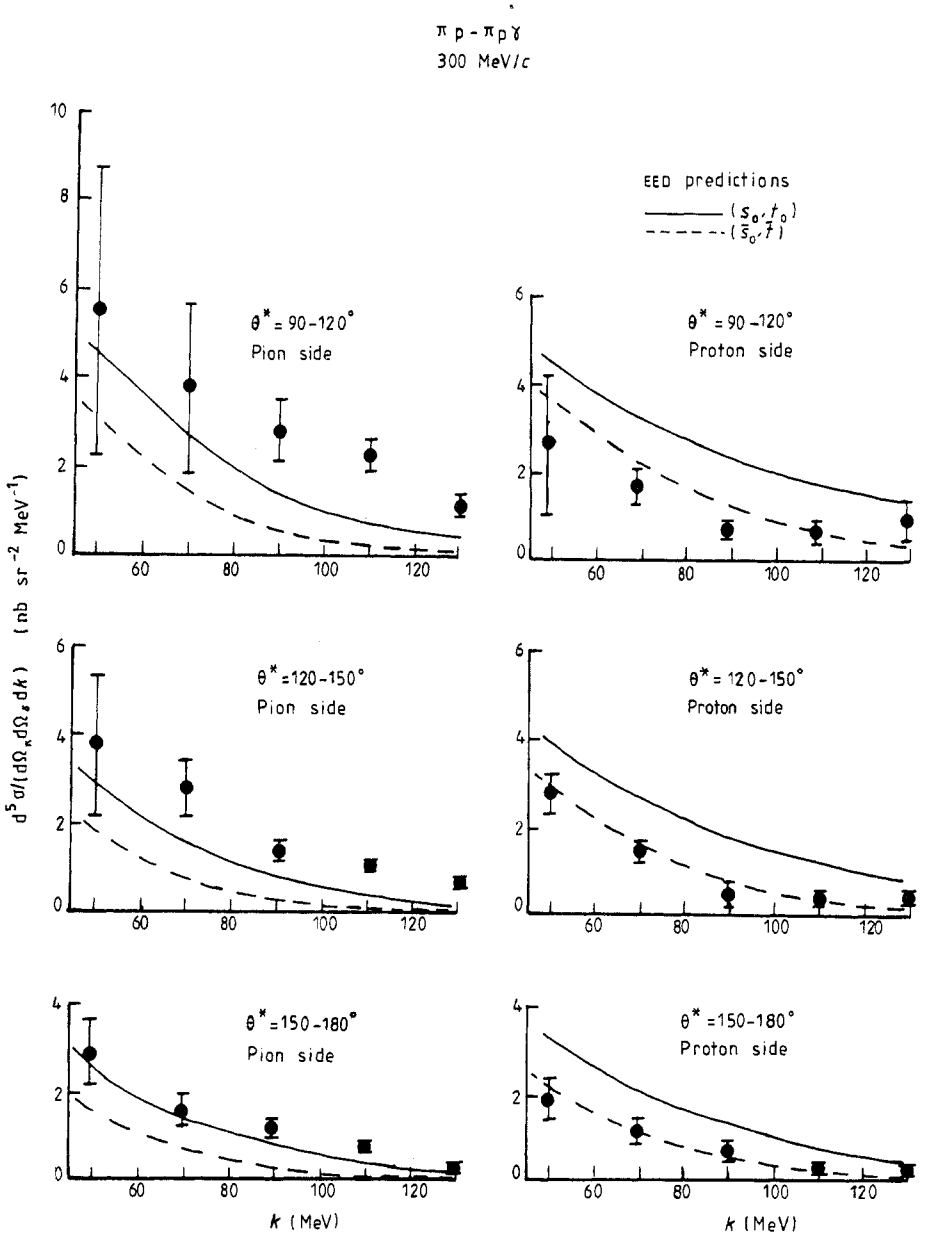

Figure 8. Bremsstrahlung cross sections from the present experiment. The cross sections, energies and angles are in CM coordinates. Also shown are EED calculations for two possible choices of the variables s and t.

variables, the geometrical restrictions in this case give implicit constraints on the five photon and pion parameters, and, in fact, restrict the particle solid angles to a rather small fraction of 4π (<10% for each arm). Thus the quoted cross section can be defined as

$$\left(\frac{\mathrm{d}^5\sigma}{\mathrm{d}\Omega_\pi^*\,\mathrm{d}\Omega_\gamma^*\,\mathrm{d}k}\right)_{\text{average}} = \int\int \frac{\mathrm{d}^5\sigma}{\mathrm{d}\Omega_\pi^*\,\mathrm{d}\Omega_\gamma^*\,\mathrm{d}k}\,\mathrm{d}\Omega_\pi^* \Big/ \int\int \mathrm{d}\Omega_\pi^*$$

where the integrals are taken over the useful acceptance of the detectors which is defined by the limits (angles in degrees)

$$\begin{aligned} &10° < \theta_\pi < 66° \\ &\theta_\mathrm{p} < 45° \\ &|\varphi_\pi| < 37(1 + \cos^{2\frac{3}{2}}\theta_\pi) \\ &|\varphi_\mathrm{p} - 180°| < 40(1 + 2\cos^{4\frac{3}{2}}\theta_\mathrm{p}) \end{aligned} \tag{2}$$

where the range of $(\theta_\pi, \varphi_\pi)$ gives explicit limits on the integrals and that of $(\theta_\mathrm{p}, \varphi_\mathrm{p})$ implicit limits. The four limits are defined in equation (2) in laboratory coordinates since they can be defined more precisely this way. The z axis is chosen along the direction of the incident beam, and the x axis is in the median plane on the side of the pion detectors.

The limits on φ_π and φ_p are convenient algebraic approximations to the acceptance limits of the detectors. However, the θ_p and θ_π limits are chosen within the geometrical acceptance to exclude events close to the elastic region ($\theta_\mathrm{p} \sim 50°$, $\theta_\pi \sim 58°$) since the tail from the elastic region gives a substantial background to the bremsstrahlung data.

The following procedure was adopted for extracting cross sections. The angular range was divided into six bins defined by $\theta_\gamma^* = 90$–$120°$, 120–150°, 150–180° for 'pion side' ($\varphi_\gamma^* < 90°$ or $\varphi_\gamma^* > 270°$) or 'proton side' ($90° < \varphi_\gamma^* < 270°$). For each bin, a scatter plot similar to figure 6 was made. In most cases, the background, assessed from the density of events away from the photon line, was negligible or was small enough that it could be estimated with confidence by assuming a constant background density across the plot. After background subtraction, the events were sorted into 20 MeV bins and converted into cross sections using the beam flux and efficiency factors described in § 3. The acceptance was calculated by generating Monte-Carlo events and subjecting them to the same analysis procedures and geometrical cuts as the data events. For $\theta_\gamma^* < 90°$ the acceptance was too small to extract cross sections.

The resulting cross sections are shown in figure 8 and table 2. The errors shown are mainly statistical but in a few cases (primarily the data for $\theta_\gamma^* = 90$–$120°$, pion side) the

Table 2. π^-p bremsstrahlung cross sections at p_π(lab.) = 301 MeV/c. Cross sections quoted are $\mathrm{d}^5\sigma/\mathrm{d}\Omega_\pi\,\mathrm{d}\Omega_\gamma\,\mathrm{d}k$ in nb sr^{-2} MeV^{-1} in centre-of-mass coordinates for the geometry described in the text.

	φ_γ^*	Pion side			Proton side		
k (MeV)	θ_γ^*	90–120°	120–150°	150–180°	90–120°	120–150°	150–180°
40–60		5.4 ± 3.3	3.7 ± 1.6	2.8 ± 0.9	2.6 ± 1.6	2.7 ± 0.5	1.8 ± 0.5
60–80		3.7 ± 2.0	2.7 ± 0.6	1.5 ± 0.4	1.6 ± 0.4	1.4 ± 0.3	1.1 ± 0.3
80–100		2.7 ± 0.8	1.3 ± 0.2	1.11 ± 0.24	0.64 ± 0.10	0.45 ± 0.25	0.65 ± 0.18
100–120		2.2 ± 0.3	0.95 ± 0.12	0.69 ± 0.17	0.61 ± 0.23	0.35 ± 0.12	0.15 ± 0.08
120–140		1.07 ± 0.19	0.58 ± 0.09	0.20 ± 0.13	0.9 ± 0.5	0.38 ± 0.16	0.20 ± 0.09

uncertainty in the shape of the background distribution contributes to the error. Systematic errors due to uncertainties in the pion flux and in the efficiency of the analysis procedure, discussed in § 3, are estimated at 15%, which is always smaller than the statistical errors. The results represent a total of 808 bremsstrahlung events.

5. Discussion

The cross sections at all angles decrease with increasing energy, following roughly the $1/k$ dependence for low photon energies, which is characteristic of bremsstrahlung cross sections.

There is little point in presenting a comparison of the present results with published theoretical models that have been applied to the UCLA data partly because, as discussed in § 1, all of these models have proved unsatisfactory to some extent, and also because theoretical work is currently in progress on further developments to these earlier treatments. In fact, a recent calculation by Picciotto [25] has already shown how part of the present data can be fitted reasonably by a modification to the procedure for establishing gauge invariance in the calculation.

To establish a comparison with other data, however, calculations are shown in figure 8 of the predictions of the external emission dominance model [14]. This model, in which just the first term of the Low expansion of the bremsstrahlung amplitude is taken, has little theoretical justification, but nevertheless it has been found give a relatively good fit to bremsstrahlung data in several cases (see § 1). If this is interpreted to indicate that bremsstrahlung is always dominated by the lowest order in k and that higher-order terms are overpredicted by most calculations, then it is of interest to see how universally the EED model applies.

In the EED model, the bremsstrahlung cross section is given by

$$\frac{\mathrm{d}^5\sigma}{\mathrm{d}\Omega_\pi\,\mathrm{d}\Omega_\gamma\,\mathrm{d}k}=\frac{e^2}{2(2\pi)^3}\,\frac{\sqrt{s}}{p'_\pi}\,\frac{p^3_{\pi'}k}{p'^2_\pi(\sqrt{s}-k)+E_{\pi'}(\boldsymbol{p}_{\pi'}\cdot\boldsymbol{k})}\,A^\mu A_\mu\left(\frac{\mathrm{d}\sigma}{\mathrm{d}\Omega}\right)_{\text{elastic}}.$$

Here, A^μ is given by

$$A^\mu=\frac{p^\mu_\pi}{\boldsymbol{p}_\pi\cdot\boldsymbol{k}}-\frac{p^\mu_\mathrm{p}}{\boldsymbol{p}_\mathrm{p}\cdot\boldsymbol{k}}-\frac{p^\mu_{\pi'}}{\boldsymbol{p}_{\pi'}\cdot\boldsymbol{k}}+\frac{p^\mu_{\mathrm{p}'}}{\boldsymbol{p}_{\mathrm{p}'}\cdot\boldsymbol{k}}$$

k is the photon four-momentum. The quantity $(\mathrm{d}\sigma/\mathrm{d}\Omega)_{\text{elastic}}$ is the π–p elastic scattering cross section. The calculation requires the elastic cross section as a function of the Lorentz invariants s and t. For the bremsstrahlung case these can be defined in several ways. For example, the values for the initial state energy and the pion momentum transfer,

$$s_0=(p_\pi+p_\mathrm{p})^2$$

$$t_0=(p_\pi-p_{\pi'})^2$$

can be taken. Alternatively, average values can be used

$$\bar{s}=\tfrac{1}{2}[(p_\pi+p_\mathrm{p})^2+(p'_\pi+p'_\mathrm{p})^2]$$

$$\bar{t}=\tfrac{1}{2}[(p_\pi-p_{\pi'})^2+(p_\mathrm{p}-p_{\mathrm{p}'})^2]$$

The predictions for these two assumptions are shown by the full and broken curves respectively in figure 8.

Clearly, both prescriptions give at least a qualitative fit to the results, as was found in the case of the UCLA data. There is no strong preference for either of the two prescriptions for s and t. However, as discussed above, there is no real theoretical justification for the EED model. The relatively good fit found here is evidence for problems in treating the higher terms in the Low expansion and, in agreement with the UCLA data, is inconsistent with models that predict large enhancements for high-energy photons. It can be hoped that the new approaches, for example by Picciotto and by the MIT group, will result in better understanding of the bremsstrahlung process.

Acknowledgments

We would like to thank John Harvey for assistance during the measurements. We would also like to thank the Rutherford Appleton Laboratory for a research grant and for the provision of computing facilities. One of us (SMP) is grateful to the SERC for a research studentship.

References

[1] Arman M, Blasberg D J, Haddock R P, Leung K C, Nefkens B M K, Schrock B L, Sober D I and Sperinde J M 1972 *Phys. Rev. Lett.* **29** 962
[2] Sober D I, Arman M, Blasberg D J, Haddock R P, Leung K C, Nefkens B M K, Schrock B L and Sperinde J M 1975 *Phys. Rev.* D **11** 1017
[3] Leung K C, Arman M, Ballagh H C, Glodis P F, Haddock R P, Nefkens B M K and Sober D I 1976 *Phys. Rev.* D **14** 698
[4] Nefkens B M K, Arman M, Ballagh H C, Glodis P F, Haddock R P, Leung K C, Smith D E A and Sober D I 1978 *Phys. Rev.* D **18** 3911
[5] Smith D E A, Glodis P F, Haddock R P, Leung K C and Tamor M A 1980 *Phys. Rev.* D **21** 1715
[6] Low F E 1958 *Phys. Rev.* **110** 974
[7] Liou M K and Nutt W T 1977 *Phys. Rev.* D **16** 2176
Liou M K 1978 *Phys. Rev.* D **18** 3390
[8] Picciotto C 1969 *Phys. Rev.* **185** 1761
[9] Picciotto C 1975 *Nuovo Cimento* A **29** 41
[10] Picciotto C 1975 *Nucl. Phys.* B **89** 357
[11] Kontratyuk L A and Ponomarev L A 1968 *Sov. J. Nucl. Phys.* **7** 82
[12] Fischer W E and Minkowski P 1972 *Nucl. Phys.* B **36** 519
[13] Pascual P and Tarrach R 1978 *Nucl. Phys.* B **134** 133
[14] Nefkens B M K and Sober D I 1976 *Phys. Rev.* D **14** 2434
[15] Picciotto C 1985 *Phys. Rev.* C **31** 1036: 1984 private communication
[16] Moniz E J 1985 private communication
[17] Zephat A G *et al* 1987 *J. Phys. G: Nucl. Phys.* submitted for publication
[18] Tanner N W 1976 *SIN Topical Meeting on Intermediate Energy Physics, Zuoz*
[19] Allardyce B W 1975 *Nuclear and Particle Physics at Intermediate Energies* ed. J B Warren (New York: Plenum) p 369
[20] van Doesburg W 1981 *PhD Thesis* Vrije Universiteit Amsterdam
[21] Playfer S M 1981 *PhD Thesis* University of Birmingham
[22] Zavrtanik D, Sever F, Pleško M, Mušič M, Kernel G, Tanner N W, Michaelis E G and Stanovnik A 1984 *Nucl. Instrum. Methods* **227** 237
[23] Chiavassa E, Costa S, Dellacasa G, Gallio M, Musso A, Panighini M, Bressani T, Bos K, van Doesburg W, Stanovnik A and Vranic D 1978 *Nucl. Instrum. Methods* **156** 187
[24] Dellacasa G, Gallio M, Musso A, Rapetti M, Zephat A G, Mirfakhrai N, Playfer S M and Michaelis E G 1980 *Nucl. Instrum. Methods* **176** 363
[25] Picciotto C 1987 *J. Phys. G: Nucl. Phys.* **13** L23